Energy and Environmental Science

ARTICLE

Biomimetic Mitochondrial Nanostructures Boost Battery Performance

Received 00th January 20xx,
Accepted 00th January 20xx

DOI: 10.1039/x0xx00000x

www.rsc.org/

Aqsa Yasmin[a,b], Muhammad A. Shehzad[a,b], Xiang Ding[a], Miaomiao Deng[a], Jiaying Liao[a], Qiao Hu[a], Xiaodong He[a], Shuo Wang[a], and Chunhua Chen[a,*]

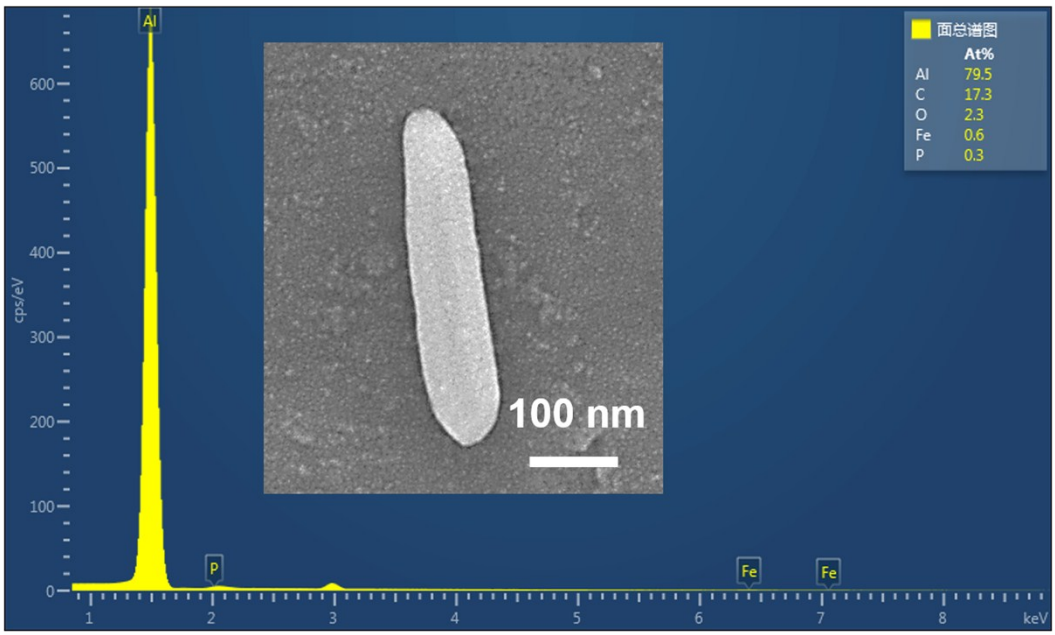

Fig. S1. SEM mapping for the region containing single MMC-LFP nanostructure.

[a.] *CAS Key Laboratory of Materials for Energy Conversions, Collaborative Innovation Centre of Suzhou Nano Science and Technology, Department of Materials Science and Engineering, School of Chemistry and Materials Science, University of Science and Technology of China, Hefei 230026, China*

[b.] *Advanced Materials and Membrane Technology Centre, Department of Polymer and Process Engineering, University of Engineering and Technology Lahore, G.T. Road-54890, Punjab Pakistan*

†Electronic Supplementary Information (ESI) available: Fig. S1 & S2, Table S1 & S2, and additional details. See DOI: 10.1039/x0xx00000x

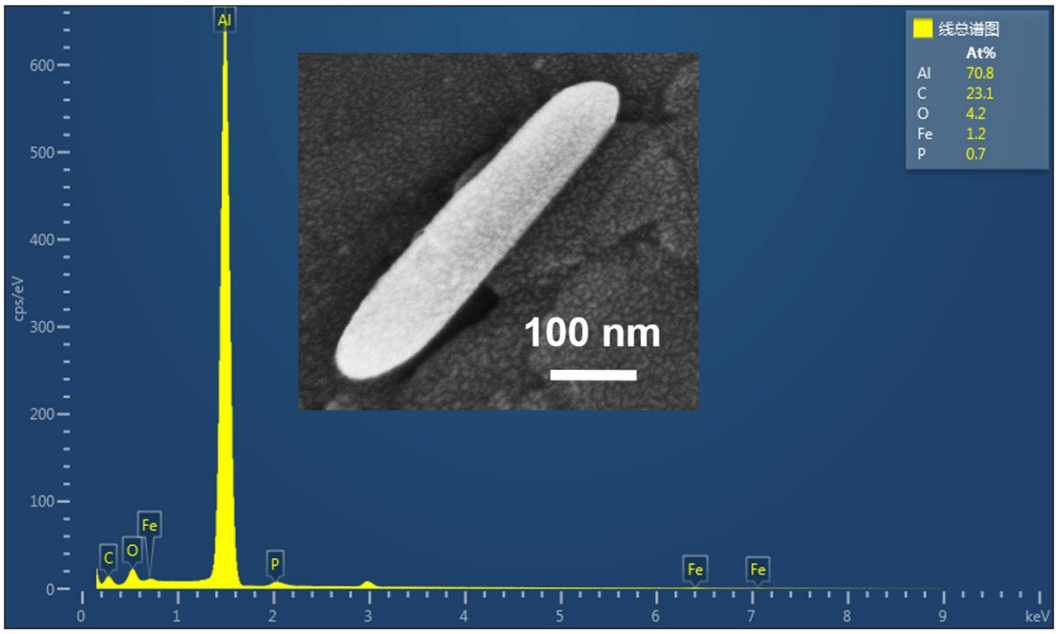

Fig. S2. SEM mapping for the region containing single DMC-LFP nanostructure.

Table S1. The simulated values of the electrical equivalent circuit elements at Fig. 3b for both the MMC- and DMC-LFP as active material. The simulation of electrochemical impedance spectroscopy (EIS) data showed more than 97.1 % and 97.5 % of fitting accuracy for the MMC-LFP and DMC-LFP containing batteries, respectively.

Circuit elements	**MMC-LFP**		**DMC-LFP**	
	Fitted value	Real standard fitting error (%)	Fitted value	Real standard fitting error (%)
$R_{S,}$ (Ω cm^2)	3.042	2.323	2.585	2.287
$Q_{Y,}$ (S·cm^{-2} s^n)	1.563E-5	1.377	9.215E-5	1.056
Q_n	0.8215	0.6786	0.9752	0.8271
$R_{ct,}$ (Ω cm^2)	75.09	0.869	61.04	0.8308
W (S·cm^{-2} s^n)	0.11147	1.792	0.01294	1.847

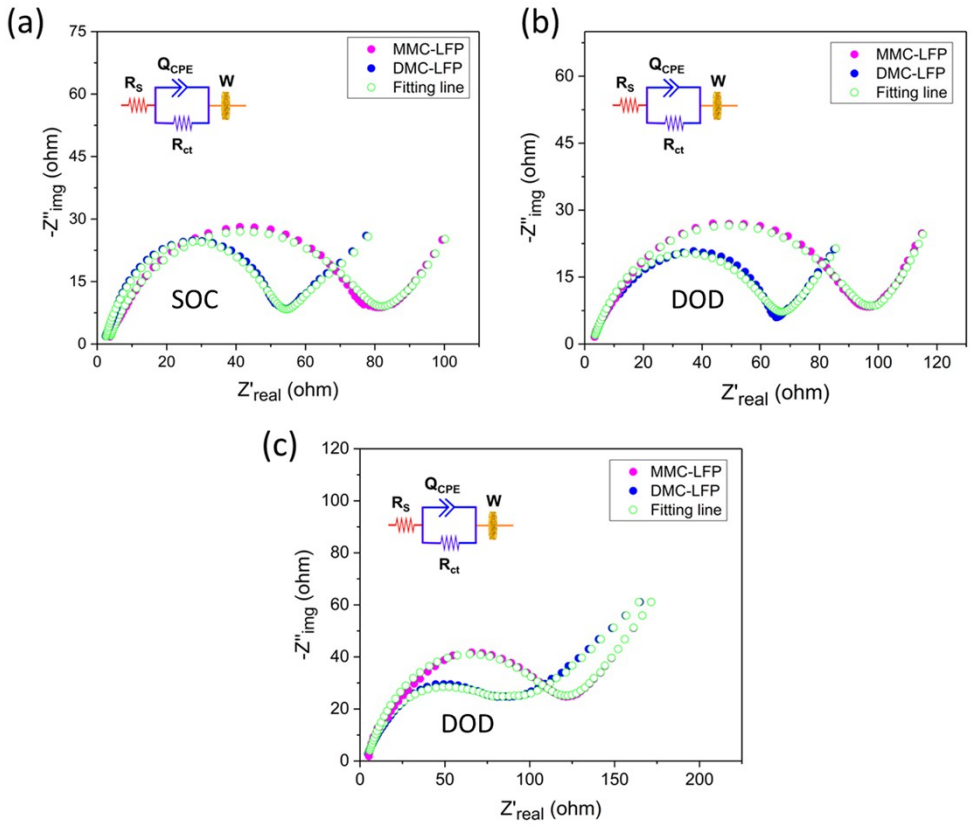

Fig. S3. EIS Nyquist spectra at different charge-discharge states for both the MC-LFP samples. (**a**) The EIS Nyquist spectra of the coin cells, individually containing MMC- and DMC-LFP, which are tested after five cycles at 0.1 C at fully charged state, whereas (**b**) at fully discharged state. (**c**) The EIS Nyquist spectra of the coin cells at fully discharge state after 1000 cycles at 10C. The fitted-simulated values for a - c are given in Table S2 - S4, respectively.

Table S2. The simulated values of the electrical equivalent circuit elements fitted at Fig. S3a.

Circuit elements	**MMC-LFP**		**DMC-LFP**	
	Fitted value	Real standard fitting error (%)	Fitted value	Real standard fitting error (%)
R_S, (Ω cm^2)	3.94	3.14	2.56	7.85
Q_Y, (S·cm^{-2} s^n)	1.137E-5	5.601	1.18E-5	4.79
Q_n	0.7789	0.6939	0.756	1.83
R_{ct}, (Ω cm^2)	81	0.9005	54	0.72
W (S·cm^{-2} s^n)	0.10357	4.899	0.01362	3.229

Table S3. The simulated values of the electrical equivalent circuit elements fitted at Fig. S3b.

Circuit elements	MMC-LFP		DMC-LFP	
	Fitted value	Real standard fitting error (%)	Fitted value	Real standard fitting error (%)
R_S, (Ω cm^2)	4.03	3.281	3.78	7.85
Q_Y, (S·cm^{-2} s^n)	1.136E-5	8.132	1.176E-5	14.79
Q_n	0.7512	1.059	0.8	1.845
R_{ct}, (Ω cm^2)	100	1.807	69.95	2.434
W (S·cm^{-2} s^n)	0.13062	2.429	0.01501	4.665

Table S4. The simulated values of the electrical equivalent circuit elements fitted at Fig. S3c.

Circuit elements	MMC-LFP		DMC-LFP	
	Fitted value	Real standard fitting error (%)	Fitted value	Real standard fitting error (%)
R_S, (Ω cm^2)	5.03	3.2	4.75	7.8
Q_Y, (S·cm^{-2} s^n)	1.136E-5	8.1	1.176E-5	14.056
Q_n	0.7512	1.05	0.769	1.8
R_{ct}, (Ω cm^2)	128	1.8	94	2.4
W (S·cm^{-2} s^n)	0.92154	2.4	0.132	4.6

Calculations for diffusion coefficients:

The diffusion coefficient of Li^+ ion (D_{Li^+}) at different charged-discharged states of the coin cells was evaluated according to the following Eq. 1.[1,2]

$$D_{Li}^{+} = \frac{1}{2}\left[\left(\frac{V_M}{AF\sigma w}\right)\frac{\delta E}{\delta x}\right]^2 \qquad (1)$$

where V_M the molar volume, *F* the Faraday constant, *A* the contact area of electrode film and electrolyte, *δE/δx* the slope of charge-discharge voltage curve and σw the Warburg coefficient determined from the EIS analysis at different charging states of the coin cells.

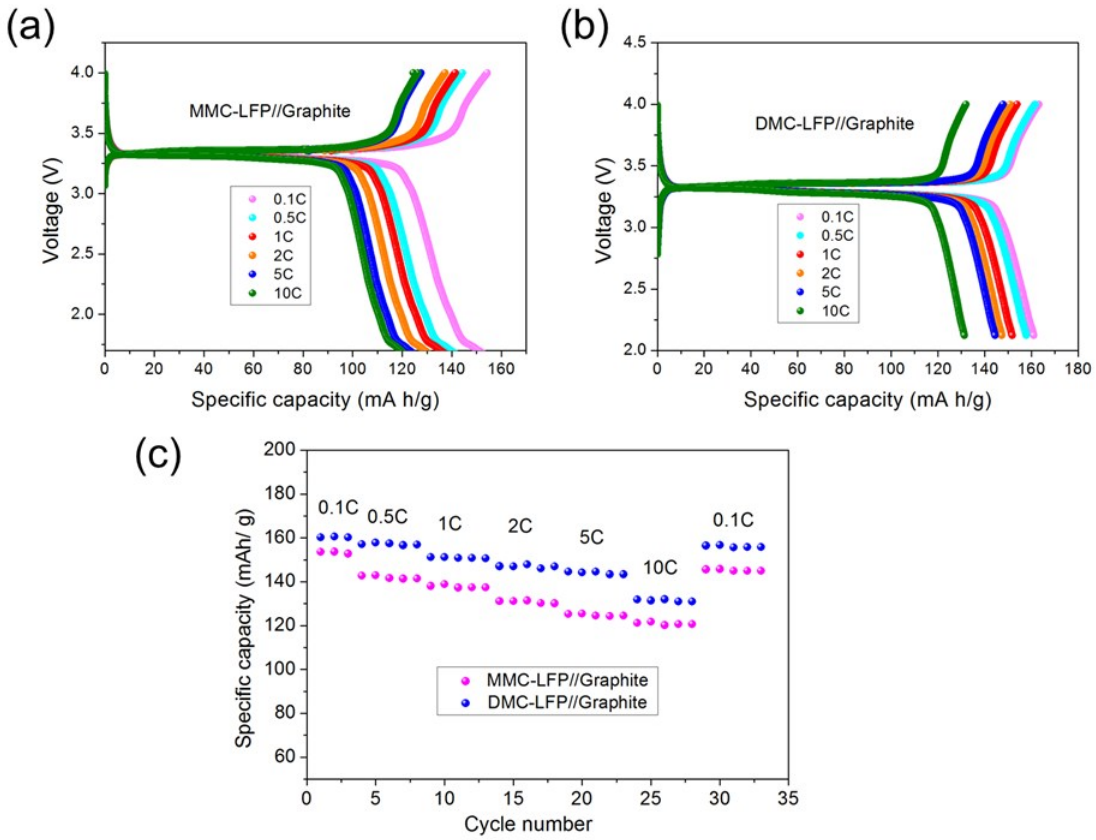

Fig. S4. Full cell characteristics of both MMC- and DMC-LFP samples. First charging-discharging cycles at different current densities for coin cell cells containing (**a**) MMC-LFP and (**b**) DMC-LFP, respectively. (**c**) The rate performance of both the materials at different current densities ranging from 0.1C to 10C.

Table S5 Comparison with recently published work infer a simultaneously improved initial reversible capacities and charge-discharge capacity retention for the dually-carbon-layered mitochondrial LFP (DMC-LFP).

Materials	Rate capability	Discharge capacity retention	References
LFP@C/G	112.3 mA h/g at 10C	500 cycles, 92%	3
LFP/G (N,S-G)	106.1 mA h/g at 10C	500 cycles, 95%	4
LFP/rGO	142 mA h/g at 0.5C	500 cycles, 90%	5
LFP/PVA	143.4 mA h/g at 5C	500 cycles, 100%	6
BCP-templated LFP/C	117 mA h/g at 20C	1000 cycles at 1C, 92%	7
LiFePO4@C/rGO	112.4 mA h/g at 10C	700 cycles 10C, 95%	8
LiFePO4/PPy/CRGO	112.1 mA h/g at 10C	500 cycles at 1C, 90.2%	9
LFP coated with polydopamine and GO	121 mA h/g at 10C	700 cycles, 96.2%	10
Nano porous $LiFePO_4$	123 mA h/g at 10C	500 cycles,	11
LFP nanocomposite	166 mA h/g at 0.1C	100 cycles, ~100%	12
LFP nanoparticles	120.9 mA h/g at 10C	500 cycles at 5C, 99.5%	13
DMC-LFP	138 mA h/g at 10C	1000 cycles, 93%	Our work

Supplementary References

1. X. Ding, L. N. Xiao, Y. X. Li, Z. F. Tang, J. W. Wan, Z. Y. Wen and C. H. Chen, *J. Power Sources*, 2018, **390**, 13-19.
2. S. Watanabe, M. Kinoshita, T. Hosokawa, K. Morigaki and K. Nakura, *J. Power Sources*, 2014, **258**, 210-217.
3. X. F. Wang, Z. J. Feng, J. T. Huang, W. Deng, X. B. Li, H. S. Zhang and Z. H. Wen, *Carbon*, 2018, **127**, 149-157.
4. J. Alam, L. A. Dass, M. S. Alhoshan and A. W. Mohammad, *Adv. Polym. Tech.*, 2013, **32**, E189-E197.
5. S. Borgmann, A. Schulte, S. Neugebauer and W. Schuhmann, in *Advances in Electrochemical Science and Engineering*, Wiley-VCH Verlag GmbH & Co. KGaA, 2012, 1-83.

6. J. C. Sun, Z. F. Li, X. Ren, L. Wang and G. C. Liang, *J. Alloys Compd.*, 2019, **773**, 788-795.

7. M. G. Fischer, X. Hua, B. D. Wilts, E. Castillo-Martinez and U. Steiner, *ACS Appl. Mater. Interfaces*, 2018, **10**, 1646-1653.

8. J. K. Holt, *Adv. Mater.*, 2009, **21**, 3542-3550.

9. S. Feng, W. Z. Shen and S. W. Guo, *J. Solid State Electrochem.*, 2017, **21**, 3021-3028.

10. J. Oh, J. Lee, T. Hwang, J. M. Kim, K.-d. Seoung and Y. Piao, *Electrochim. Acta*, 2017, **231**, 85-93.

11. J. Liu, T. E. Conry, X. Song, M. M. Doeff and T. J. Richardson, *Energy Environ. Sci.*, 2011, **4**, 885-888.

12. J. Yang, J. Wang, Y. Tang, D. Wang, X. Li, Y. Hu, R. Li, G. Liang, T.-K. Sham and X. Sun, *Energy Environ.Sci.*, 2013, **6**, 1521-1528.

13. Y. Wang, X. Wang, J. Li, Z. Mo, X. Zhao, X. Jing and F. Wang, *Adv. Mater.*, 2001, **13**, 1582-1585